Sensorless Induction Motor Drive Using Modified Integral Sliding Mode Control-Based MRAS

Hau Huu Vo

Modeling Evolutionary Algorithms Simulation and Artificial Intelligence, Faculty of Electrical and Electronics Engineering, Ton Duc Thang University, Ho Chi Minh City, Vietnam (e-mail: vohuuhau@tdtu.edu.vn).

Abstract: A modified integral sliding mode control-based adaptation algorithm (MISMCA) is described to enhance performance of sensorless rotor flux based model reference adaptive system (RF-MRAS) induction motor drive (IMD). At low speed regions, performance of RF-MRAS is not guaranteed due to conventional PI-based adaptation algorithm (PIA) and parameter uncertainties, especially rotor time constant. In order to improve performance of RF-MRAS, the PIA is replaced by an algorithm based on integral sliding mode control (ISMC). In the ISMC design, the term that contains rotor time constant is considered as noise, and a reference model-based approximation is employed to adapt rotor time constant. Moreover, bipolar sigmoid function is utilized to reduce chattering-phenomenon. Simulations with sensorless RF-MRAS direct torque control IMD confirm the advantages of the MISMCA compared with the PIA in terms of maximum value and ITAE index of estimated speed error.

Keywords: integral sliding mode control (ISMC), rotor flux-model reference adaptive system (RF-MRAS), sensorless control, induction motor drive (IMD), direct torque control (DTC).

1. INTRODUCTION

Sensorless methods provide some advantages such as reduction of installation and maintainance cost, complexity of hardware, increases of mechanical robustness, working capability in hostile environments (Vas, 1998). The term "sensorless" means that induction motor drive (IMD) does not own the speed or position sensor in its control structure, and the concept of sensorless control is to utilize estimation algorithms to get rotor speed or rotor position or flux from motor terminals currents and voltages (Bose, 2002). Sensorless control techniques have increased reliability of IMD systems based on vector control or direct torque control (DTC) (Holtz, 2002). Various techniques such as model reference adaptive system (MRAS) (Schauder, 1992), Luenberger observer (Luenberger, 1971), sliding mode observer (SMO) (Lascu et al., 2004), extended Kalman filter (Kim et al., 1994), artificial neural network method (Maiti et al., 2012) were widely utilized. Several listed techniques were combined together or modified to improve IMD systems' performance (Holakooie et al., 2016; Zhang et al., 2020).

Among listed techniques, MRAS variations were also developed (Benlaloui et al., 2015; Das et al., 2019; Özdemir, 2020) or enhanced by other techniques (Gadoue et al., 2010; Kavuran et al., 2017; Tarchała and Orłowska-Kowalska, 2018; Reddy et al., 2020; Vo et al., 2020). The MRAS based on electromagnetic torque and rotor flux was developed from conventional MRAS or rotor flux-based MRAS (RF-MRAS) (Benlaloui et al., 2015). Sensorless control using difference between the stator d- and q-circuits' effective working was presented (Das et al., 2019). Output voltage of q-axis current regulator and its estimate were considered reference model and adaptive model respectively (Özdemir, 2020). Conventional PIA in RF-MRAS was replaced by two adaptation algorithms (Gadoue et al., 2010). The MRAS was combined with modified fractional order integrator to enhance tracking performance (Kavuran et al., 2017). Equivalent signal technique was utilized to reduce chattering-phenomenon in stator current-based MRAS (SC-MRAS) with sliding mode control (SMC) (Tarchała and Orłowska-Kowalska, 2018). Stator currents were compensated to decrease speed error tracking in reference model of the SC-MRAS (Reddy et al., 2020). Parameters of the PIA in the SC-MRAS were updated by fuzzy logic in sensorless IMD utilizing pulse width modulation-DTC (PWM-DTC) (Vo et al., 2020).

In MRAS variations above, the RF-MRAS provided poor performance in comparison to others, for example presence of parameter sensitivity, and bad performance at low speed area (Özdemir, 2020). The SMC has been a commonly-used method in design of robust controllers or observers. For improvement, the conventional PIA in the RF-MRAS is replaced by integral SMC (ISMC) (Gadoue et al., 2010; Pan et al., 2018; Tarchała and Orłowska-Kowalska, 2018; Ullah et al., 2019; Zhang et al., 2020; Ahmadi et al., 2022; Sharma et al., 2022; Lumertz et al., 2023). Switching function (SF) candidate of this RF-MRAS is a function of signal error calculated from rotor fluxes (Gadoue et al., 2010) instead of stator currents (Zhang et al., 2020), or both rotor fluxes and stator currents (Tarchała and Orłowska-Kowalska, 2018). Global asymptotic stability was guaranteed in ISMC design, and the ISMC controlled both the dynamics of the nonlinear system and the disturbances (Ullah et al., 2019). However, utilization of sign function brought high frequency chattering-phenomenon (Gadoue et al., 2010) and it is necessary to redesign for reduction. In order to lower chattering, low-pass filter (LPF) and an integral sliding variable were employed (Pan et al., 2018). Parameter of the LPF must be properly chosen to reduce chattering-phenomenon and not present delay of speed estimation (Tarchała and Orłowska-Kowalska, 2018). Another solution was utilization of a term that adapted to SF variation and system states (Zhang et al., 2020). The ISMC design utilized the super-twisting approach to decrease the chattering (Ahmadi et al., 2022). The combination between the ISMC and the state observer provided the avoidance of using large gain for switching function (Sharma et al., 2022). The switching function was replaced by smooth functions to reduce the chattering (Lumertz et al., 2023). Along with the reduction of the chattering-phenomenon, it is necessary to estimate or approximate rotor time constant (Toliyat et al., 2003) because its accuracy heavily affects the performance of the RF-MRAS. Many functional candidates such as rotor fluxes, stator voltages, active power, reactive power were utilized to estimate rotor time constant based on MRAS (Cao et al., 2017).

Section 2 describes sensorless PWM-DTC IMD using RF-MRAS. With the aim of performance improvement of sensorless RF-MRAS IMD at low speed region in operations including starting (ST), forward motoring (FM), forward braking (FB), reverse motoring (RM), reverse braking (RB), unloading (UL), design of proposed ISMC adaptation algorithm is presented. In this design, sign function is replaced with bipolar sigmoid one for decreasing high-frequency ripple of numerator of speed estimate, and an approximation function based on stator current and rotor flux of reference model instead of adaptive model is utilized to obtain rotor time constant. Section 3 shows simulation results. Conclusions are carried out in final section.

LIST OF SYMBOLS

f_s	switching frequency of the inverter
i_{sa}, i_{sb}	phase-a, phase-b stator currents
$i_{s\alpha}, i_{s\beta}$	stator current components in stator frame
$\mathbf{i}_s = i_{s\alpha} + j i_{s\beta}$	stator current vector
J_m	moment of inertia
L_m	magnetizing inductance
L_s, L_r	stator and rotor inductances
p	number of pole pairs
R_s, R_r	stator and rotor resistances
T_e	motor torque
T_L	load torque
$T_r = {}^{L_r}/_{R_r}$	nominal rotor time constant
$\tilde{T}_r$	real rotor time constant
$\hat{T}_r$	estimated rotor time constant
$t_s = {}^{1}/_{f_s}$	switching period of the inverter
t_0	fundamental sample time used for numerical methods in simulation software
$u_{s\alpha}, u_{s\beta}$	stator voltage components in stator frame
$\mathbf{u}_s = u_{s\alpha} + j u_{s\beta}$	stator voltage vector
u_{sx}^*, u_{sy}^*	reference stator voltage components in stator flux frame
$u_{s\alpha}^*, u_{s\beta}^*$	reference values of $u_{s\alpha}, u_{s\beta}$
$\mathbf{u}_s^* = u_{s\alpha}^* + j u_{s\beta}^*$	reference stator voltage vector
γ	orienting angle
η	coefficient designed for desired chattering region of the switching function
ξ	adaptive signal
$\psi_{s\alpha}, \psi_{s\beta}$	stator flux components in stator frame
$\boldsymbol{\psi}_s = \psi_{s\alpha} + j\psi_{s\beta}$	stator flux vector
ψ_s	stator flux vector magnitude
ψ_s^*	reference stator flux magnitude
$\psi_{r\alpha}, \psi_{r\beta}$	rotor flux components in stator frame
$\boldsymbol{\psi}_r = \psi_{r\alpha} + j\psi_{r\beta}$	rotor flux vector
$\hat{\psi}_{r\alpha}, \hat{\psi}_{r\beta}$	estimated values of $\psi_{r\alpha}, \psi_{r\beta}$
$\hat{\boldsymbol{\psi}}_r = \hat{\psi}_{r\alpha} + j\hat{\psi}_{r\beta}$	estimate of $\boldsymbol{\psi}_r$
ω_m	mechanical rotor speed
$\omega_{m,ref}$	reference mechanical rotor speed
$\hat{\omega}_m$	estimated mechanical rotor speed
$\omega_r = p\omega_m$	electrical rotor speed
$\hat{\omega}_r$	estimated electrical rotor speed

2. PROPOSED ISMC ADAPTATION ALGORITHM FOR SENSORLESS RF-MRAS IMD

Figure 1 shows sensorless PWM-DTC IMD associated with RF-MRAS speed estimator. Signal Calculation block provides three important signals of PWM-DTC according to (1)-(5) (Brandstetter et al., 2017):

$$\frac{d\psi_{s\alpha}}{dt} = u_{s\alpha} - R_s i_{s\alpha} \tag{1}$$

$$\frac{d\psi_{s\beta}}{dt} = u_{s\beta} - R_s i_{s\beta} \tag{2}$$

$$\psi_s = \sqrt{\psi_{s\alpha}^2 + \psi_{s\beta}^2} \tag{3}$$

$$\gamma = sin^{-1}\left(\frac{\psi_{s\beta}}{\psi_s}\right) \tag{4}$$

$$T_e = 1.5p\left(i_{s\beta}\psi_{s\alpha} - i_{s\alpha}\psi_{s\beta}\right) \tag{5}$$

Flux and torque controllers that are PI controllers, utilize errors of stator flux $\Delta\psi_s$ and motor torque ΔT_e to respectively output reference stator voltage components in stator flux frame u_{sx}^* and u_{sy}^*. Vector Rotation block employs these components and orienting angle γ to obtain reference values $u_{s\alpha}^*, u_{s\beta}^*$ of stator voltage components in stator frame.

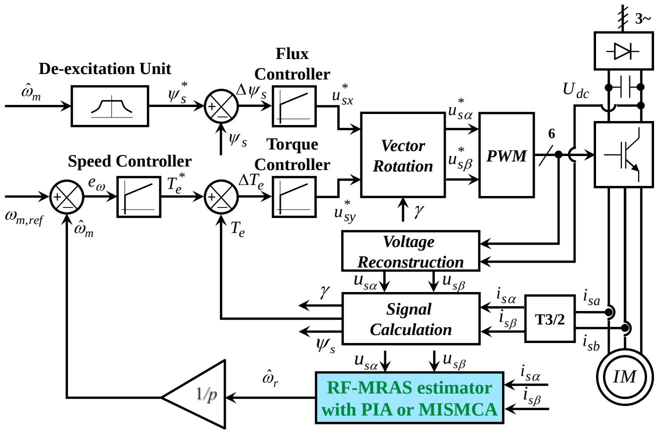

Fig. 1. Sensorless IMD utilizing RF-MRAS speed estimator.

The PWM block calculates switch-on and switch-off durations of solid-state devices of the inverter in one switching period. Estimated electrical rotor speed-feedback signal of controlled system, is computed by RF-MRAS estimator with PIA or proposed MISMCA (see Figure 2). For the RF-MRAS, reference model and adaptive model which are voltage model and current model are utilized to calculate rotor flux components and their estimates, according to (6)-(7) and (8)-(9) respectively (Bose, 2002):

$$\psi_{r\alpha} = \frac{L_r}{L_m}\left[\int \left(u_{s\alpha} - R_s i_{s\alpha}\right)dt - \left(\frac{L_s L_r - L_m^2}{L_r}\right) i_{s\alpha}\right] \tag{6}$$

$$\psi_{r\beta} = \frac{L_r}{L_m}\left[\int \left(u_{s\beta} - R_s i_{s\beta}\right)dt - \left(\frac{L_s L_r - L_m^2}{L_r}\right) i_{s\beta}\right] \tag{7}$$

$$\hat{\psi}_{r\alpha} = \int \left(-\frac{1}{T_r}\hat{\psi}_{r\alpha} - \hat{\omega}_r \hat{\psi}_{r\beta} + \frac{L_m}{T_r} i_{s\alpha}\right) dt \tag{8}$$

$$\hat{\psi}_{r\beta} = \int \left(\hat{\omega}_r \hat{\psi}_{r\alpha} - \frac{1}{T_r}\hat{\psi}_{r\beta} + \frac{L_m}{T_r} i_{s\beta}\right) dt \tag{9}$$

In case of the PIA (see Figure 2a), adaptive signal ξ is computed by (10), and according to Appendix C, it is minimized thanks to Popov's theorem for getting the estimated electrical rotor speed by (11):

$$\xi = \psi_{r\beta}\hat{\psi}_{r\alpha} - \psi_{r\alpha}\hat{\psi}_{r\beta} \tag{10}$$

$$\hat{\omega}_r = k_{p,est}\left(\xi + \frac{1}{T_{i,est}}\int_0^t \xi dt\right) \tag{11}$$

where $k_{p,est} > 0, T_{i,est} > 0$ are proportional gain and integral constant time.

For the MISMCA (see Figure 2b), there are three modifications including utilization of ISMC to minimize the adaptive signal, application of bipolar sigmoid function to reduce the chattering-phenomenon, and approximation of rotor time constant to provide exact information for the RF-MRAS.

Switching function S which is utilized to switch the adaptive signal ξ and its time derivative, are expressed by (12)-(13) (Gadoue et al., 2010):

$$S = \xi + k_{ss}\int_0^t \xi dt \tag{12}$$

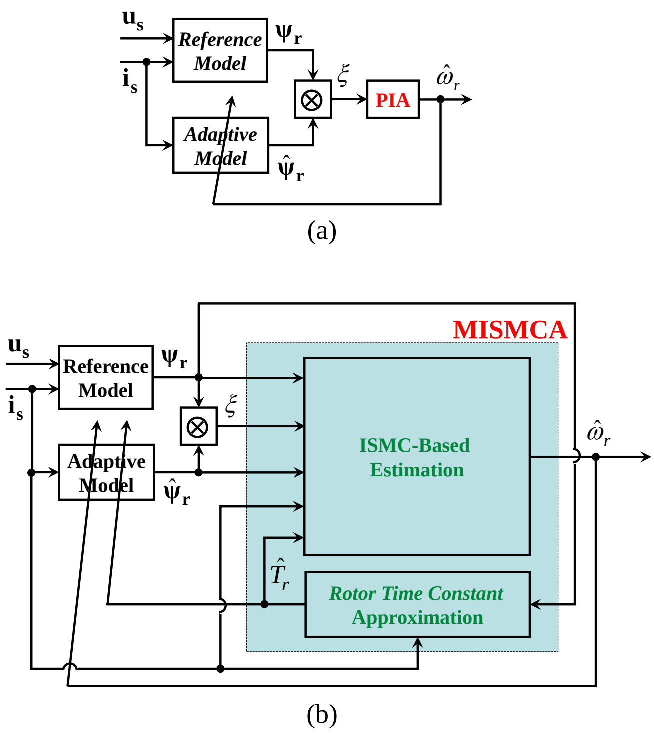

Fig. 2. RF-MRAS speed estimator (a) with the PIA (b) with the MISMCA.

$$\dot{S} = \dot{\xi} + k_{ss}\xi \tag{13}$$

where $k_{ss} > 0$. From (10), the time derivative of the adaptive signal is computed as follows:

$$\dot{\xi} = \psi_{r\beta}\dot{\hat{\psi}}_{r\alpha} + \hat{\psi}_{r\alpha}\dot{\psi}_{r\beta} - \psi_{r\alpha}\dot{\hat{\psi}}_{r\beta} - \hat{\psi}_{r\beta}\dot{\psi}_{r\alpha} \tag{14}$$

Estimated rotor flux components in (8)-(9) are differentiated, and substituted into (14) to get (15):

$$\begin{aligned}\dot{\xi} = &-\left(\psi_{r\alpha}\hat{\psi}_{r\alpha} + \psi_{r\beta}\hat{\psi}_{r\beta}\right)\hat{\omega}_r \\ &+\left(\hat{\psi}_{r\alpha}\dot{\psi}_{r\beta} - \hat{\psi}_{r\beta}\dot{\psi}_{r\alpha}\right) \\ &-\frac{1}{T_r}\left(\psi_{r\beta}\hat{\psi}_{r\alpha} - \psi_{r\alpha}\hat{\psi}_{r\beta}\right) + \frac{L_m}{T_r}\left(\psi_{r\beta} i_{s\alpha} - \psi_{r\alpha} i_{s\beta}\right)\end{aligned} \tag{15}$$

Next, Lyapunov theory is employed to derive the estimated electrical rotor speed. At first, Lyapunov function candidate is defined by (16):

$$V = \frac{1}{2}S^2 \tag{16}$$

Its time derivative is expressed by (17):

$$\dot{V} = S\dot{S} \tag{17}$$

The estimator is stable when the candidate function approaches 0. This will be achieved if the function $\dot{V}$ is negative definite. In order to guarantee the negative definition of the function $\dot{V}$, the function $\dot{S}$ must satisfy following condition:

$$\dot{S} < 0 \; for \; S > 0$$

$$\dot{S} > 0 \; for \; S < 0$$

$$\dot{S} = 0 \; for \; S = 0 \tag{18}$$

An imposition is carried out:

$$\dot{S} = -k_f\sigma(S) + f_n \tag{19}$$

where:

$$\sigma(S) = \tanh\left(\frac{\eta S}{2}\right) \tag{20}$$

$$\eta = -\frac{ln\frac{S_0}{2 - S_0}}{S_0} \tag{21}$$

k_f and f_n are quantities to be calculated, S_0 is small positive, and $[-S_0, S_0]$ is desired chattering region of the switching function.

By replacing (10), (15) and (19) into (13), the estimated electrical rotor speed is simplified as follows:

$$\widehat{\omega}_r = \frac{f_c + f_o - f_n}{f_d} \tag{22}$$

where:

$$f_c = k_f\sigma(S) + \left(\widehat{\psi}_{r\alpha}\dot{\psi}_{r\beta} - \widehat{\psi}_{r\beta}\dot{\psi}_{r\alpha}\right) \tag{23}$$

$$f_o = \frac{(k_{ss}T_r - 1)\xi + L_m\left(\psi_{r\beta}i_{s\alpha} - \psi_{r\alpha}i_{s\beta}\right)}{T_r} \tag{24}$$

$$f_d = \psi_{r\alpha}\widehat{\psi}_{r\alpha} + \psi_{r\beta}\widehat{\psi}_{r\beta} \tag{25}$$

We adopt:

$$f_n = f_o \tag{26}$$

From equations (22) and (26), the desired formula (27) is obtained:

$$\widehat{\omega}_r = \frac{f_c}{f_d} \tag{27}$$

Equations (18) and (19) lead to:

$$k_f = \begin{cases} \dfrac{f_o}{\sigma(S)} + \varepsilon \; for \; \sigma(S) > 0 \\ unchanged \; for \; \sigma(S) = 0 \\ \dfrac{f_o}{\sigma(S)} - \varepsilon \; for \; \sigma(S) < 0 \end{cases} \tag{28}$$

These conditions indicate that the switching function will go to sliding line $S = 0$ and stay on it if both the adaptive signal and the motor torque are zero.

Rotor time constant T_r needs to be approximated because of changes of IM's working condition. In Figure 2, Rotor Time Constant Approximation (RTCA) block online estimates T_r to provide Adaptive Model and ISMC-Based Estimation blocks (see Figure 2). Differentiating (8)-(9), and converting yield:

$$\dot{\widehat{\psi}}_{r\alpha} = \frac{L_m i_{s\alpha} - \widehat{\psi}_{r\alpha}}{T_r} - \widehat{\omega}_r\widehat{\psi}_{r\beta} \tag{29}$$

$$\dot{\widehat{\psi}}_{r\beta} = \frac{L_m i_{s\beta} - \widehat{\psi}_{r\beta}}{T_r} + \widehat{\omega}_r\widehat{\psi}_{r\alpha} \tag{30}$$

In order to eliminate the $\widehat{\omega}_r$, multiplying (32), (33) by $\widehat{\psi}_{r\alpha}, \widehat{\psi}_{r\beta}$ respectively, adding them together, and then converting the sum yields:

$$T_r = \frac{\left(L_m i_{s\alpha} - \widehat{\psi}_{r\alpha}\right)\widehat{\psi}_{r\alpha} + \left(L_m i_{s\beta} - \widehat{\psi}_{r\beta}\right)\widehat{\psi}_{r\beta}}{\widehat{\psi}_{r\alpha}\dot{\widehat{\psi}}_{r\alpha} + \widehat{\psi}_{r\beta}\dot{\widehat{\psi}}_{r\beta}} \tag{31}$$

Utilizing (34) makes T_r approximation incorrect because the adaptive model contains T_r (see (8) and (9)). Assume that the adaptive model goes to the reference model with the designed control law, rotor time constant is approximated by (35):

$$\widehat{T}_r = \frac{(L_m i_{s\alpha} - \psi_{r\alpha})\psi_{r\alpha} + \left(L_m i_{s\beta} - \psi_{r\beta}\right)\psi_{r\beta}}{\psi_{r\alpha}\dot{\psi}_{r\alpha} + \psi_{r\beta}\dot{\psi}_{r\beta}} \tag{32}$$

Equation (32) can cause a sudden change in the T_r approximation, which leads to a sudden one in $\widehat{\psi}_{r\alpha}, \widehat{\psi}_{r\beta}, \dot{\xi}$ (see (8), (9), (15) respectively) and then a spike in the estimated electrical rotor speed ((23), (25) and (27)) as T_r changes from initialized nominal value to real value. The LPF (33) is utilized to overcome this problem:

$$G_{LPF}(s) = \frac{1}{\tau s + 1} \tag{33}$$

where τ is time constant of the filter, and $\widehat{T}_r(0) = T_r$. Implemenations of the RTCA and ISMC-Based Estimation blocks are shown in Figures 3 and 4. Note that the equations (24), (26) and (28) use $\widehat{T}_r$ instead of T_r, and the z^{-1} block in Figure 4 works with discretization step of $t_s = 5 \times 10^{-5}(s)$ – switching period of the inverter to ensure the calculation precision. Depending on capability of hardware used for simulation or realistic implementation, it must be chosen as small as possible to minimize the chattering phenomenon.

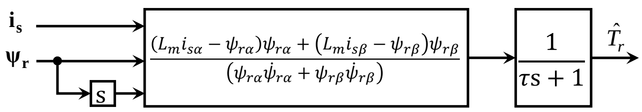

Fig. 3. Implementation of the RTCA block.

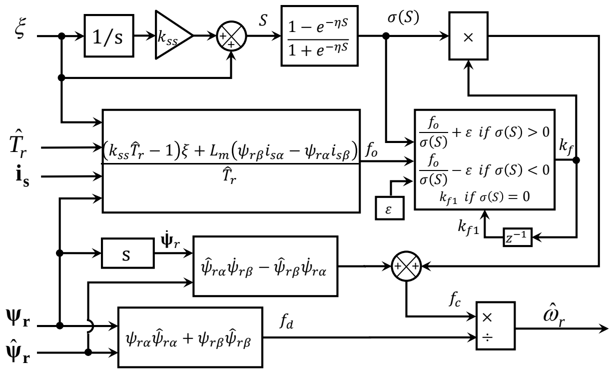

Fig. 4. Implementation of the ISMC-Based Estimation block.

3. SIMULATION RESULTS

Sensorless DTC drives utilizing the RF-MRAS with the PIA and the MISCMA are simulated in case of $k_{ss} = 0.7143$, parameters listed in Appendix B. In case of the SVPWM technique, $t_0 = t_s/20$ is fundamental sample time used for numerical methods in simulation software. Simulations are implemented at load torque diagram with the jump of 5N·m and reference mechanical rotor speeds of $10\pi/3(rad/s)$ and $\pi/3(rad/s)$ which respectively represent for low-speed region (LSR) and very-low-speed region (VLSR). The PI controllers including the PIA, torque, flux, speed controllers, are anti windup PI ones. In all simulations, initial value of rotor time constant is the nominal one.

In order to evaluate each operation of the sensorless drives, maximum absolute of difference between mechanical rotor speed and its estimate $M_{est,n}$ is normalized as follows:

$$M_{est,n} = \frac{max|e_{est}|}{max|\omega_{m,ref}|} \tag{34}$$

where

$$e_{est} = \omega_m - \widehat{\omega}_m \tag{35}$$

And for the evaluation of all IM operations, normalized integral of time multiply by absolute error (ITAE) index is proposed as follows:

$$ITAE_{est,n} = \frac{\int_0^2 t|e_{est}|dt}{max|\omega_{m,ref}|} \tag{36}$$

In case of $\tilde{T}_r = T_r$, mechanical rotor speed, motor torque, difference between mechanical rotor speed and its estimate, adaptive signal for low-speed and very-low-speed regions are respectively shown in Figures 5-8. In the figures, there are drive operations including ST (0.0s-0.4s), FM (0.4s-0.7s), FB (0.7s-1.0s), RM (1.0s-1.4s), RB (1.4s-1.7s), UL (1.7s-2.0s). Values of $M_{est,n}$ listed in Table 1 show that MISMCA brings higher estimation accuracy than PIA, reducing on average 93% at value for both LSR and VLSR. Table 2 indicates that MISMCA respectively dedicates 18.5 times and 25 times smaller $ITAE_{est,n}$ than PIA at LSR and VLSR. The reason for this is the MISMCA brings the switching function very close to zero and low chattering, leading to the adaptive signal for MISMCA (see Figure 9) closer to zero than the adaptive signal for PIA (see Figure 8). However, chattering problem has not been eliminated (see Figure 7).

The smaller estimate indices $M_{est,n}$ and $ITAE_{est,n}$ are associated lower overshoot/undershoot (see Table 3) and shorter settling time (see Table 4) of mechanical rotor speed response for MISMCA, decreasing on average 27% and 36% in overshoot/undershoot compared to PIA at LSR and VLSR, respectively. Torque responses (Figure 6) for MISCMA contain much less oscillations than for PIA. Reason for this is responses of difference between mechanical rotor speed and its estimate (Figure 7), and of adaptive signal (Figure 8) for PIA have higher magnitudes than for MISMCA, especially at times of change of IM operations.

Figures 10-11 show rotor time constant estimation processes with and without the LPF, and speed responses in cases of $\tilde{T}_r = 1.5T_r$ and $\tilde{T}_r = 0.5T_r$. It is easy to see that there are fluctuations in starting operation, especially at case of $\tilde{T}_r = 0.5T_r$ (see Figure 11). Without the LPF in the RTCA block, estimate of rotor time constant is changed suddenly. This makes the time derivative of the adaptive signal greater, and the estimated speed more fluctuated than compared to the case with the LPF (see Figure 12).

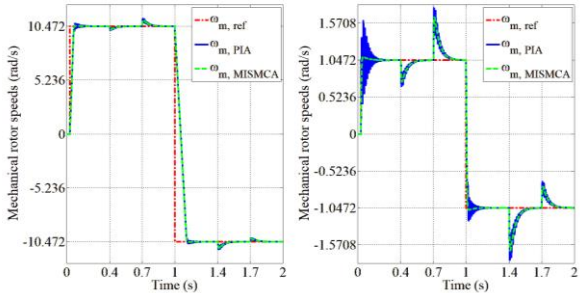

Fig. 5. Mechanical rotor speed responses at LSR (left), and VLSR (right).

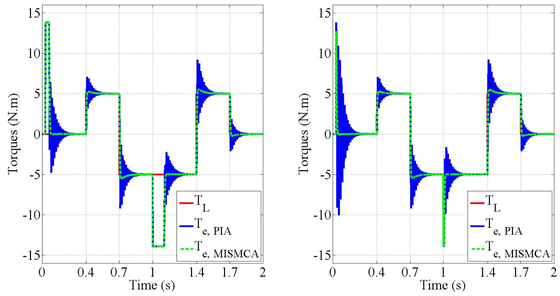

Fig. 6. Torques at LSR (left), and VLSR (right).

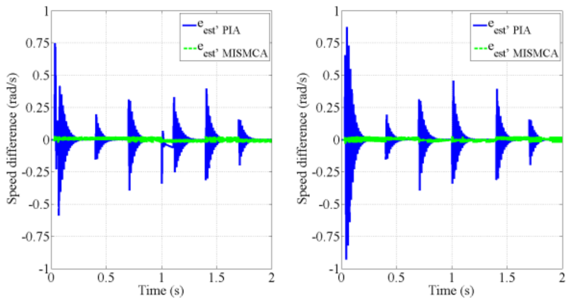

Fig. 7. Speed differences at LSR (left), and VLSR (right).

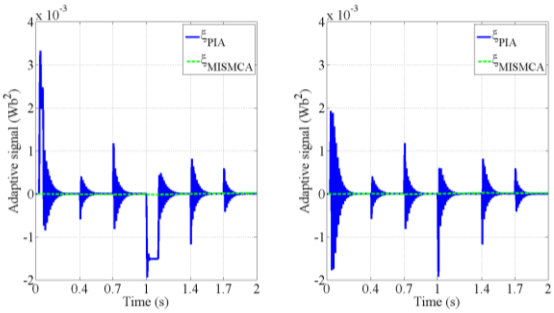

Fig. 8. Adaptive signals at LSR (left), and VLSR (right).

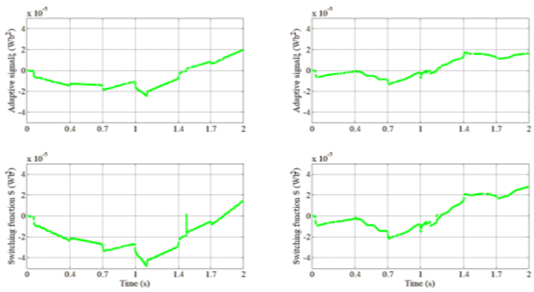

Fig. 9. Switching function and adaptive signal at LSR (left), and VLSR (right).

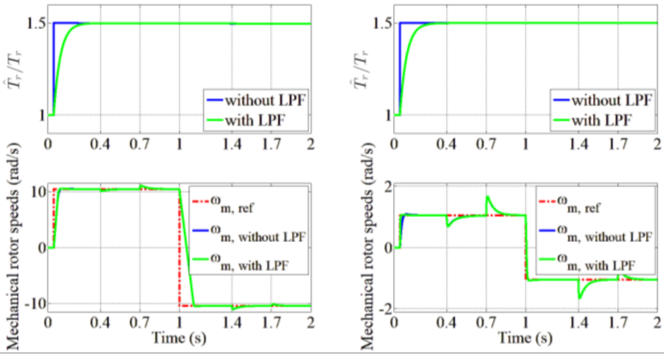

Fig. 10. Rotor time constant estimation and mechanical rotor speed responses at LSR (left), and VLSR (right), $\tilde{T}_r = 1.5T_r$.

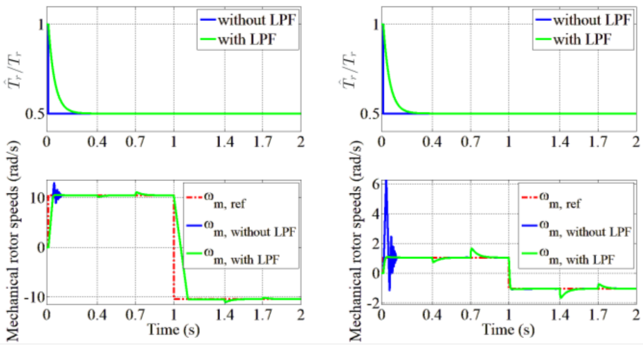

Fig. 11. Rotor time constant estimation and mechanical rotor speed responses at LSR (left), and VLSR (right), $\tilde{T}_r = 0.5T_r$.

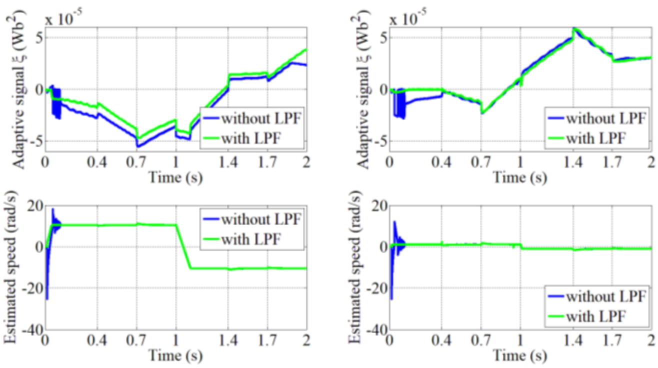

Fig. 12. Adaptive signal and estimated mechanical rotor speeds at LSR (left), and VLSR (right), $\tilde{T}_r = 0.5T_r$.

Table 1. $M_{est,n}$ **(%) at LSR and VLSR.**

IM operation	LSR		VLSR	
	PIA	MISMCA	PIA	MISMCA
ST	7.2	0.26	88.8	3.0
FM	1.9	0.23	18.6	2.2
FB	3.8	0.24	37.6	2.2
RM	3.2	0.25	43.6	2.5
RB	3.8	0.23	37.5	2.5
UL	1.9	0.21	18.8	2.3

Table 2. $ITAE_{est,n}$ **[$\times 10^{-3}s^2$] at LSR and VLSR.**

Region	PIA	MISMCA
LSR	5.8	0.32
VLSR	53.8	2.1

Table 3. Overshoot/Undershoot (%) at LSR and VLSR.

IM operation	LSR		VLSR	
	PIA	MISMCA	PIA	MISMCA
ST	2.5	0.5	53.2	4.6
FM	3.5	2.9	35.2	29.2
FB	7.1	5.8	70.6	58.1
RM	1.6	0.3	17.2	2.9
RB	7.1	5.9	70.6	58.1
UL	3.5	2.9	35.2	28.9

Table 4. Settling time (s) at LSR and VLSR.

IM operation	LSR		VLSR	
	PIA	MISMCA	PIA	MISMCA
ST	0.096	0.068	0.186	0.095
FM	0.437	0.431	0.539	0.537
FB	0.766	0.763	0.868	0.868
RM	1.118	1.111	1.136	1.049
RB	1.466	1.463	1.568	1.568
UL	1.736	1.731	1.837	1.838

4. CONCLUSIONS

The adaptation algorithm using ISMC with bipolar sigmoid function was presented to replace the one using PI controller in RF-MRAS speed estimator of sensorless induction drive. Proposed adaptive algorithm guaranteed Lyapunov stability of RF-MRAS estimator, dedicated chattering-phenomenon reduction and high adaptation to large uncertainty up to ± 50% of nominal rotor time constant. The algorithm excellently improves the poor performance of the RF-MRAS based on conventional PI one. It brought significantly lower normalized estimated speed error and ITAE than the conventional adaptive algorithm, especially at VLSR with normalized ITAE indice reduced by 96% compared to conventional one. Due to its simple computation, proposed sensorless control structure can be implemented on real control systems with digital signal processors at switching frequency greater than or equal to 3kHz (Tarchała and Orłowska-Kowalska, 2018; Das et al., 2019; Vo et al., 2020; Bărbulescu et al., 2023). SMC techniques such as high order method or super-twisting algorithm can be utilized to get more accurate estimated electrical rotor speed. Adaptive methods can be employed to update the parameter τ of the low-pass filter in the rotor time constant estimation.

REFERENCES

Ahmadi, B., Xie, W.-F., and Zakeri, E. (2022). Robust Cascade Vision/Force Control of Industrial Robots Utilizing Continuous Integral Sliding-Mode Control Method. *IEEE/ASME Transactions on Mechatronics*, 27(1), 524–536.

Bărbulescu, C., Căiman, D.V., et al. (2023). Implementation of Parameter Observer for Capacitors. *Sensors*, 23(2), p.948.

Benlaloui, I., Drid, S., et al. (2015). Implementation of a New MRAS Speed Sensorless Vector Control of Induction Machine. *IEEE Transactions on Energy Conversion*, 30(4), 588-595.

Bose, B.K. (2002). *Modern Power Electronics and AC Drives*, ch. 8. Prentice Hall, New Jersey.

Brandstetter, P., Kuchar, M., et al. (2017). Induction motor drive with PWM direct torque control. In Stanislav Rusek, Radomir Gono (ed.), *Proceedings of the 2017 18th International Scientific Conference on Electric Power Engineering (EPE)*, 409–413. IEEE, New York.

Cao, P., Zhang, X., and Yang, S. (2017). A Unified-Model-Based Analysis of MRAS for Online Rotor Time Constant Estimation in an Induction Motor Drive. *IEEE Transactions on Industrial Electronics*, 64(6), 4361–4371.

Das, S., Kumar, R., and Pal, A. (2019). MRAS-Based Speed Estimation of Induction Motor Drive Utilizing Machines' d- and q-Circuit Impedances. *IEEE Transactions on Industrial Electronics*, 66(6), 4286–4295.

Gadoue, S.M., Giaouris, D., and Finch, J.W. (2010). MRAS Sensorless Vector Control of an Induction Motor Using New Sliding-Mode and Fuzzy-Logic Adaptation Mechanisms. *IEEE Transactions on Energy Conversion*, 25(2), 394–402.

Holakooie, M.H., Ojaghi, M., and Taheri. A. (2016). Full-order Luenberger observer based on fuzzy-logic control for sensorless field-oriented control of a single-sided linear induction motor. *ISA Transactions*, 60, 96–108.

Holtz, J. (2002). Sensorless Control of Induction Motor Drives. *Proceedings of the IEEE*, 90(8), 1359–1394.

Kavuran, G., Ates, A., et al. (2017). An Experimental Study on Model Reference Adaptive Control of TRMS by Error-Modified Fractional Order MIT Rule. *Control Engineering and Applied Informatics*, 19(4), 101–111.

Khalil, H.K. (2002). *Nonlinear Systems*, ch.6-7. Pearson, New Jersey.

Kim, Y.R., Sul, S.K., and Park, M.H. (1994). Speed sensorless vector control of an induction motor using an extended Kalman filter. *IEEE Transactions on Industry Applications*, 30(5), 1225–1233.

Lascu, C., Boldea, I., and Blaabjerg, F. (2004). Direct torque control of sensorless induction motor drives: a sliding-mode approach. *IEEE Transactions on Industry Applications*, 40(2), 582–590.

Landau, Y.D. (1979). *Adaptive Control – The Model Referencing Approach*. Marcel Dekker.

Luenberger, D. (1971). An introduction to observers. *IEEE Transactions on Automatic Control*, 16(6), 596–602.

Lumertz, M.M., dos Santos, S.T.C.A., et al. (2023). Performance-based design of pseudo-sliding mode speed control for electrical motor drives. *Control Engineering Practice*, 132, 105413.

Maiti, S., Verma, V., et al. (2012). An Adaptive Speed Sensorless Induction Motor Drive With Artificial Neural Network for Stability Enhancement. *IEEE Transactions on Industrial Informatics*, 8(4), 757–766.

Özdemir, S. (2020). A New Stator Voltage Error-Based MRAS Model for Field-Oriented Controlled Induction Motor Speed Estimation Without Using Voltage Transducers. *Electrical Engineering*, 102(4), 2465–2479.

Pan, Y., Yang, C., et al. (2018). Integral Sliding Mode Control: Performance, Modification, and Improvement. *IEEE Transactions on Industrial Informatics*, 14(7), 3087–3096.

Popov, V.M. (1973). *Hyperstability of Control Systems*. Springer Berlin Heidelberg, Berlin.

Reddy, C.U., Prabhakar, K.K., et al. (2020). Speed Estimation Technique Using Modified Stator Current Error-Based MRAS for Direct Torque Controlled Induction Motor Drives. *IEEE Journal of Emerging and Selected Topics in Power Electronics*, 8(2), 1223–1235.

Schauder, C. (1992). Adaptive Speed Identification for Vector Control of Induction Motors without Rotational Transducers. *IEEE Transactions on Industrial Electronics*, 28(5), 1054–1061.

Sharma, A., Alturki, A., and Amrr, S. M. (2022). Extended State Observer Based Integral Sliding Mode Control for Maglev System With Fixed Time Convergence. *IEEE Access*, 10, 93074–93083.

Tarchała, G. and Orłowska-Kowalska, T. (2018). Equivalent-Signal-Based Sliding Mode Speed MRAS-Type Estimator for Induction Motor Drive Stable in the Regenerating Mode. *IEEE Transactions on Industrial Electronics*, 65(9), 6936–6947.

Toliyat, H.A., Levi, E., and Raina, M. (2003). A review of RFO induction motor parameter estimation techniques. *IEEE Transactions on Energy Conversion*, 18(2), 271–283.

Ullah, S., Khan, Q., et al. (2019). Integral backstepping based robust integral sliding mode control of underactuated nonlinear electromechanical systems. *Control Engineering and Applied Informatics*, 21(3), 42–50.

Vas, P. (1998). *Sensorless Vector and Direct Torque Control*. Oxford University Press, Oxford.

Vo, H.H., Kuchar, M., and Brandstetter, P. (2020). Application of fuzzy logic in sensorless induction motor drive with PWM-DTC, *Electrical Engineering*, 102(1), 129–140.

Zhang, Y., Yin, Z., et al. (2020). A Novel Sliding Mode Observer With Optimized Constant Rate Reaching Law for Sensorless Control of Induction Motor. *IEEE Transactions on Industrial Electronics*, 67(7), 5867–5878.

Appendix A. ACRONYMS

DTC	direct torque control
FB	forward braking
FM	forward motoring
IM	induction motor
IMD	induction motor drive
ISMC	integral SMC
ITAE	integral of time multiply by absolute error
LPF	low-pass filter
LSR	low-speed region
MISMCA	modified integral sliding mode control-based adaptation algorithm
MRAS	model reference adaptive system
PI	proportional-integral
PIA	PI-based adaptation algorithm
PWM	pulse width modulation
RB	reverse braking
RF-MRAS	rotor flux-based MRAS
RM	reverse motoring
RTCA	Rotor Time Constant Approximation
SC-MRAS	stator current-based MRAS
SF	switching function
SMC	sliding mode control
SMO	sliding mode observer
ST	starting
SVPWM	space vector PWM
UL	unloading
VLSR	very-low-speed region

Appendix B. PWM-DTC DRIVE AND IM PARAMETERS

	Parameter	Value
IM	Rated power	2.2kW
	Rated speed	1420rpm
	Rated voltage	230V/400V
	Rated torque	14.8N·m
	Number of pole pairs	$p = 2$
	Moment of inertia	$J_m = 0.0047 kg \cdot m^2$
	Stator resistance	$R_s = 3.179\Omega$
	Stator inductance	$L_s = 0.209H$
	Mutual inductance	$L_m = 0.192H$
	Rotor resistance	R_r =2.118Ω
	Rotor inductance	$L_r = 0.209H$
	Nominal rotor time constant	$T_r = 0.0987s$
Voltage source inverter	DC link voltage	540V
	Switching frequency	20kHz
	PWM technique	SVPWM
PI speed controller	Gain	1.5
	Integral time constant	0.05s
	Limits of output	±14Nm
PI flux controller	Gain	100
	Integral time constant	0.01s
PI torque controller	Gain	5
	Integral time constant	0.05s

Appendix C. APPLICATION OF POPOV'S THEOREM FOR MINIMIZING THE ADAPTIVE SIGNAL

Deriving (8)-(9) and writing the resulting equations in vector form:

$$\frac{d\hat{\boldsymbol{\psi}}_r}{dt} = \left(j\hat{\omega}_r - \frac{1}{T_r}\right)\hat{\boldsymbol{\psi}}_r + \frac{L_m}{T_r}\mathbf{i}_s \tag{C.1}$$

Assume that the reference model of the rotor flux vector is given by (C.2):

$$\frac{d\boldsymbol{\psi}_r}{dt} = \left(j\omega_r - \frac{1}{T_r}\right)\boldsymbol{\psi}_r + \frac{L_m}{T_r}\mathbf{i}_s \tag{C.2}$$

Subtract (C.1) from (C.2), and convert the resulting equation to obtain (C.3):

$$\frac{d\mathbf{x}}{dt} = \left(j\omega_r - \frac{1}{T_r}\right)\mathbf{x} + j(\omega_r - \hat{\omega}_r)\hat{\boldsymbol{\psi}}_r \tag{C.3}$$

where: $\mathbf{x} = \boldsymbol{\psi}_r - \hat{\boldsymbol{\psi}}_r$. The equation (C.3) is expressed in stator frame:

$$\frac{dx_\alpha}{dt} = -\frac{1}{T_r}x_\alpha - \omega_r x_\beta - (\omega_r - \hat{\omega}_r)\hat{\psi}_{r\beta} \tag{C.4}$$

$$\frac{dx_\beta}{dt} = \omega_r x_\alpha - \frac{1}{T_r}x_\beta + (\omega_r - \hat{\omega}_r)\hat{\psi}_{r\alpha} \tag{C.5}$$

where: $\mathbf{x} = x_\alpha + jx_\beta$.

Consider system formed by (C.6)-(C.9):

$$\frac{d\mathbf{x}}{dt} = \mathbf{A}_s\mathbf{x} + \mathbf{B}_s\mathbf{u} \tag{C.6}$$

$$\mathbf{y} = \mathbf{C}_s\mathbf{x} \tag{C.7}$$

$$\mathbf{u} = -\mathbf{w}(t) \tag{C.8}$$

$$\mathbf{w}(t) = \mathbf{f}(\mathbf{y}(\tau), t), for\ 0 \le \tau \le t \tag{C.9}$$

where:

$$\mathbf{x} = \begin{bmatrix} x_\alpha \\ x_\beta \end{bmatrix} = \begin{bmatrix} \psi_{r\alpha} - \hat{\psi}_{r\alpha} \\ \psi_{r\beta} - \hat{\psi}_{r\beta} \end{bmatrix},$$

$$\mathbf{u} = \begin{bmatrix} u_\alpha \\ u_\beta \end{bmatrix} = \begin{bmatrix} -(\omega_r - \hat{\omega}_r)\hat{\psi}_{r\beta} \\ (\omega_r - \hat{\omega}_r)\hat{\psi}_{r\alpha} \end{bmatrix}, \mathbf{y} = \begin{bmatrix} y_\alpha \\ y_\beta \end{bmatrix},$$

$$\mathbf{A}_s = \begin{bmatrix} -\frac{1}{T_r} & -\omega_r \\ \omega_r & -\frac{1}{T_r} \end{bmatrix}, \mathbf{B}_s = \begin{bmatrix} 1 & 0 \\ 0 & 1 \end{bmatrix}, \mathbf{C}_s = \begin{bmatrix} 1 & 0 \\ 0 & 1 \end{bmatrix} \quad (C.10)$$

If the system is proved to be asymptotically hyperstable, the estimated electrical rotor speed will approach the electrical rotor speed. Because the dynamics of the motor's electrical quantities are much faster than the dynamics of rotations, the electrical rotor speed is assumed to be constant. The system is a nonlinear system which is represented as a feedback connection of two subsystems: 1st subsystem - a linear *t*-invariant system is formed by (C.6)-(C.7), 2nd subsystem - a non-linear *t*-variant system is given by (C.8)-(C.9). The system will be asymptotically hyperstable when the 1st subsytem has strictly positive real transfer function matrix (Popov, 1973; Landau, 1979; Khalil, 2002). Due to $\mathbf{B}_s$ and $\mathbf{C}_s$ the 1st subsystem is both controllable and observable, the system is said to be hyperstable if conditions (C.11)-(C.12) are satisfied:

$$\forall t > 0, for\ \delta(\|\mathbf{x}(0)\|) \geq 0,$$

$$\int_0^t \mathbf{w}^T(t)\,\mathbf{y}(t)dt \geq -\delta(\|\mathbf{x}(0)\|) \sup_{0 \leq \tau \leq t} \|\mathbf{x}(\tau)\| \quad (C.11)$$

$$\forall \mathbf{x}(0), \exists K > 0, \forall t > 0,$$

$$\|\mathbf{x}(t)\| \leq K[\delta(\|\mathbf{x}(0)\|) + \|\mathbf{x}(0)\|] \quad (C.12)$$

Additionally, if condition (C.13) is satisfied

$$\lim_{t\to\infty} \mathbf{x}(t) = \mathbf{0} \quad (C.13)$$

, the system is asymptotically hyperstable (Popov, 1973; Landau, 1979; Khalil, 2002). And thereby,

$$\lim_{t\to\infty} \hat{\omega}_r(t) = \omega_r \quad (C.14)$$

The next part is to prove that the transfer function matrix of the 1st subsytem is strictly positive real and to select an electrical rotor speed estimation formula satisfying the inequality (C.11).

The 1st subsystem has transfer function matrix given by (C.15):

$$\mathbf{G}(s) = \mathbf{C}_s(s\mathbf{I} - \mathbf{A}_s)^{-1}\mathbf{B}_s = \frac{1}{s^2 + \frac{2}{T_r}s + \left(\frac{1}{T_r}\right)^2 + \omega_r^2} \begin{bmatrix} s + \frac{1}{T_r} & -\omega_r \\ \omega_r & s + \frac{1}{T_r} \end{bmatrix} \quad (C.15)$$

Auxiliary matrix $\mathbf{H}(s)$ and its determinant of the transfer function matrix are calculated as follows:

$$\mathbf{H}(s) = \mathbf{G}(s) + \mathbf{G}^T(-s) = \frac{2T_r}{[(T_r s + 1)^2 + (T_r\omega_r)^2][(T_r s - 1)^2 + (T_r\omega_r)^2]} \times \begin{bmatrix} -T_r^2 s^2 + T_r^2\omega_r^2 + 1 & 2T_r^2\omega_r s \\ -2T_r^2\omega_r s & -T_r^2 s^2 + T_r^2\omega_r^2 + 1 \end{bmatrix} \quad (C.16)$$

$$\det(\mathbf{H}(s)) = 2T_r \quad (C.17)$$

The assumption of the lemma of strictly positive real transfer function matrix (Popov, 1973; Khalil, 2002) is satisfied because the determinant is different from zero. The 1st condition of the lemma is also satisfied because all elements of $\mathbf{G}(s)$ have poles in region $Re\{s\} < 0$ (due to $T_r > 0$). Determinants of the 1st and 2nd principal minors of the $\mathbf{H}(j\omega)$ are given by (C.18) and (C.19):

$$\det(\mathbf{H}_{11}(j\omega)) = \frac{2T_r(T_r^2\omega^2 + T_r^2\omega_r^2 + 1)}{[-(T_r\omega)^2 + (T_r\omega_r)^2 + 1]^2 + 4(T_r\omega)^2} \quad (C.18)$$

$$\det(\mathbf{H}_{22}(j\omega)) = \det(\mathbf{H}(j\omega)) = 2T_r \quad (C.19)$$

Equations (C.18) and (C.19) indicate that the determinants are positive definite, resulting in the $\mathbf{H}(j\omega)$ being positive definite for any real ω. This means that the 2nd condition of the lemma (Popov, 1973; Khalil, 2002) is also fullfilled (according to Sylvestre's criteria). Matrix $[\mathbf{G}(\infty) + \mathbf{G}^T(\infty)]$ can be considered a positive semidefinite matrix because it is equal to zero. There exists such a matrix $\mathbf{M} = \mathbf{I}$ that the $\lim_{\omega\to\infty} \omega^2\mathbf{M}^T[\mathbf{G}(j\omega) + \mathbf{G}^T(-j\omega)]\mathbf{M}$ is positive definite as shown in (C.20):

$$\lim_{\omega\to\infty} \omega^2\mathbf{M}^T[\mathbf{G}(j\omega) + \mathbf{G}^T(-j\omega)]\mathbf{M} = \lim_{\omega\to\infty}\Bigg\{ \frac{2T_r\omega^2}{[(jT_r\omega + 1)^2 + (T_r\omega_r)^2][(jT_r\omega - 1)^2 + (T_r\omega_r)^2]} \times \begin{bmatrix} T_r^2\omega^2 + T_r^2\omega_r^2 + 1 & j2T_r^2\omega_r\omega \\ -j2T_r^2\omega_r\omega & T_r^2\omega^2 + T_r^2\omega_r^2 + 1 \end{bmatrix}\Bigg\} = \begin{bmatrix} \frac{2}{T_r} & 0 \\ 0 & \frac{2}{T_r} \end{bmatrix} \quad (C.20)$$

Hence, the 3rd condition of the lemma is also fulfilled, and the transfer function matrix $\mathbf{G}(s)$ is strictly positive, resulting in the 1st subsystem (C.6)-(C.7) being asymptotically hyperstable. The rest is to choose a formula of speed estimation that satisfies the condition (C.11).

The left term of the inequality in (C.11) is given by:

$$\int_0^t \mathbf{w}^T(t)\,\mathbf{y}(t)dt = \int_0^t \Big((\psi_{r\alpha}\hat{\psi}_{r\beta} - \psi_{r\beta}\hat{\psi}_{r\alpha})(\omega_r - \hat{\omega}_r)\Big)\,dt \quad (C.21)$$

In order to satisfy the condition (C.11), the estimated electrical rotor speed is selected as follows:

$$\hat{\omega}_r = \Phi_1(\mathbf{x}) + \int_0^t \Phi_2(\mathbf{x})dt \quad (C.22)$$

where:

$$\Phi_1(\mathbf{x}) = k_{p,est}\xi \quad (C.23)$$

$$\Phi_2(\mathbf{x}) = \frac{k_{p,est}}{T_{i,est}}\xi \quad (C.24)$$

$$\xi = -(\psi_{r\alpha}\hat{\psi}_{r\beta} - \psi_{r\beta}\hat{\psi}_{r\alpha}) = \psi_{r\beta}\hat{\psi}_{r\alpha} - \psi_{r\alpha}\hat{\psi}_{r\beta} \quad (C.25)$$

$k_{p,est} > 0, T_{i,est} > 0$. Substituting equations (C.22)-(C.25) into (C.21) leads to (C.26):

$$\int_0^t \mathbf{w}^T(t)\,\mathbf{y}(t)dt = k_{p,est}\int_0^t \xi^2 dt + \\ + \int_0^t \left(-\xi\left(\omega_r - \int_0^t \frac{k_{p,est}}{T_{i,est}}\xi d\tau\right)\right)dt \quad (C.26)$$

First term of the right of the equality (C.26) is always not negative. Assume that $\omega_r = const$, second term is converted and compared as follows:

$$\int_0^t \left(-\xi\left(\omega_r - \int_0^t \frac{k_{p,est}}{T_{i,est}}\xi d\tau\right)\right)dt = \\ \frac{T_{i,est}}{k_{p,est}}\int_0^t f(t)df(t) = \frac{T_{i,est}[f(t)^2 - f(0)^2]}{2k_{p,est}} \geq \\ -\frac{T_{i,est}f(0)^2}{2k_{p,est}} = -\frac{T_{i,est}\omega_r^2}{2k_{p,est}} \quad (C.27)$$

where:

$$f(t) = \omega_r - \int_0^t \frac{k_{p,est}}{T_{i,est}}\xi d\tau \quad (C.28)$$

Therefore, the inequality (C.11) is fullfilled in the electrical rotor speed estimation utilizing (C.22)-(C.25), resulting in the speed estimation being hyperstable. From equations (C.22)-(C.25) is obtained (11).